Elsevier Editorial System(tm) for CR Geoscience

Manuscript Draft

Manuscript Number: GEOSCIENCE-D-15-00161R1

Title: RECORD OF EOCENE-MIOCENE THRUSTING IN THE WESTERN AXIAL ZONE AND CHAÎNONS BÉARNAIS (WEST-CENTRAL PYRENEES) REVEALED BY MULTI-METHOD THERMOCHRONOLOGY

Article Type: Article for Thematic Issue

Keywords: Thermochronology, apatite fission tracks, apatite and zircon (U-Th)/He, thrusting, Pyrenees

Corresponding Author: Ms. Gemma V. Bosch,

Corresponding Author's Institution: Géosciences Rennes 1 and BRGM.

First Author: Gemma V. Bosch

Order of Authors: Gemma V. Bosch; Antonio Teixell; Marc Jolivet; Pierre Labaume; Daniel Stockli; Mireia Domènech; Patrick Monié

Abstract: We present new apatite (U-Th)/He (AHe), apatite fission track (AFT) and zircon (U-Th)/He) (ZHe) data to unravel the timing of exhumation and thrusting in the western Axial Zone of the Pyrenees and the adjacent North Pyrenean Zone. In the north, ZHe data yield cooling signals between 26-50 Ma in the Chaînons Béarnais, consistent with the onset of thrust-related cooling in the neighboring Mauléon basin modeled by previous authors. Non-reset Triassic ages are found in the footwall of the North Pyrenean Frontal thrust (Aquitaine basin). To the south, similar ZHe ages in both the hangingwall and footwall of the Lakora thrust record late Eocene to Oligocene cooling that we attribute to activity of the Gavarnie thrust. Thermal modeling of samples from the thrust hangingwall indicate cooling from early Eocene times, recording activity of the Lakora thrust. Paleozoic detrital samples from the westernmost Axial Zone and from the Eaux-Chaudes, Balaitous and Panticosa granitic plutons yield signals of AFT (between 20-30 Ma) and ZHe (20-25 Ma). Modeling indicate fast cooling during this time that we attribute to motion of the Guarga thrust. AHe data from these Axial Zone plutons, combined with modeling, show a post-tectonic signal (8-9 Ma) that indicates renewed erosion after a period without major cooling and exhumation between 20 to 10 Ma.

Post-print of Bosch, Gemma V. et al. «Timing of Eocene–Miocene thrust activity in the Western Axial Zone and Chaînons Béarnais (west-central Pyrenees) revealed by multi-method thermochronology» in Comptes Rendus Geoscience (Elsevier), Vol. 348, Issue 3-4 (March-April 2016), p. 246-256. The final version is available at DOI 10.1016/j.crte.2016.01.001

ABSTRACT

We present new apatite (U-Th)/He (AHe), apatite fission track (AFT) and zircon (U-Th)/He (ZHe) data to unravel the timing of exhumation and thrusting in the western Axial Zone of the Pyrenees and the adjacent North Pyrenean Zone (Chaînons Béarnais). In the north, ZHe data yield cooling signals between 26-50 Ma in the Chaînons Béarnais, consistent with the onset of thrust-related cooling in the neighboring Mauléon basin modeled by previous authors. Non-reset Triassic ages are found in the footwall of the North Pyrenean Frontal thrust (Aquitaine basin). To the south, similar ZHe ages in both the hangingwall and footwall of the Lakora thrust record late Eocene to Oligocene cooling that we attribute to activity of the Gavarnie thrust. Thermal modeling of samples from the Lakora thrust hangingwall indicate cooling from early Eocene times, recording activity of the Lakora thrust. Paleozoic detrital samples from the westernmost Axial Zone and from the Eaux-Chaudes and Balaitous-Panticosa granitic plutons yield signals of AFT between 20-30 Ma and ZHe between 20-25 Ma. Modeling indicate fast cooling during this time that we attribute to motion of the Guarga thrust. AHe data from these Axial Zone plutons, combined with modeling, show a post-tectonic signal (8-9 Ma) that indicates renewed erosion after a period without major cooling and exhumation between 20 to 10 Ma.

Key words: Thermochronology, apatite fission tracks, apatite and zircon (U-Th)/He, thrusting, Pyrenees

1. Introduction

Unraveling the timing and dynamics of mountain building is a long-standing goal in collisional orogen studies. This goal is traditionally addressed by tectonics-sedimentation analysis of synorogenic deposits and, more recently, by low-temperature thermochronology on the assumption that dated exhumation paths reflect the vertical component of the evolution of thrust belts. In the Pyrenees, the foreland basin record is well known, and thermochronologic studies have focused in the past decades on the Paleozoic massifs of the Axial Zone (Morris et al., 1998; Fitzgerald et al., 1999; Sinclair et al., 2005; Gibson et al., 2007; Jolivet et al., 2007; Maurel et al., 2008; Gunnell et al., 2009; Metcalf et al., 2009) (figure 1a). More recent thermochronologic studies have included the Cenozoic sedimentary rocks of the South Pyrenean foreland basin and the Paleozoic and Mesozoic rocks of the North Pyrenean Zone, to better constrain the relationships between the exhumation in the Axial Zone and the exhumation and burial in the adjacent basins (Meresse, 2010; Beamud et al., 2011; Whitchurch et al., 2011; Fillon and van der Beek, 2012; Fillon et al. 2013; Rushlow et al., 2013; Mouthereau et al., 2014; Vacherat et al., 2014).

While most of the thermochronologic studies focus on the eastern and east-central Pyrenees, often around the ECORS-Pyrenees profile, the western Axial Zone and adjoining areas have been less investigated. To understand the relationships between the exhumation in the Axial Zone and the dynamics of the fold and thrust belt in the forelands, the western Axial Zone gives key information; this part of the basement massif interacts to the south with the Tertiary Jaca basin, which contains the most complete foreland basin sequence recording the structural development (e.g. Cámara and Klimowitz, 1985; Labaume et al., 1985; Barnolas and Teixell, 1994; Teixell and García-Sansegundo, 1995; Teixell, 1996; Millán et al., 2000).

This work presents the first multi-method thermochronology database of the western Axial Zone of the Pyrenees (figure 1a), including apatite fission track (AFT), (U-Th)/He in zircon (ZHe) and apatite (AHe) data, with the aim to investigate the Pyrenean (Cenozoic) evolution. A few samples of the adjacent North Pyrenean Zone (Chaînons Béarnais area) are also included in the study. The area investigated is particularly interesting because it comprises the western termination of the Axial Zone massif where it plunges under Upper Cretaceous and Paleogene rocks. It also constitutes the only area where we can observe the Cretaceous North Pyrenean basin overthrusting the Southern Pyrenees (Teixell, 1990, 1998). The thermochronology data obtained are compared with the tectonostratigraphic record of the foreland basins and integrated in the tectonic framework of the west-central Pyrenees, providing a more complete picture of the history of thrust uplift and exhumation (syn-tectonic and post-tectonic) of this segment of the chain.

2. Geological setting

The Pyrenees formed from late Cretaceous to early Miocene times due to convergence between the Iberian and European continental margins (Choukroune et al., 1990; Muñoz, 1992). As a result of the collision, the west-central Pyrenees rose as a doubly-verging orogenic prism built by basement and cover-involved thrusts. This collision belt is underlain by north-directed lower crustal subduction (Teixell, 1998; Lagabrielle et al., 2010; Teixell et al. this volume). The main upper crustal structures of this segment of the chain are shown in figure 1b. The North Pyrenean Zone was a rapidly-subsiding Cretaceous basin between the European and Iberian margins, floored by hyper-thinned continental crust and exhumed mantle from Albian-Cenomanian times (Lagabrielle et Bodinier, 2008; Jammes et al., 2009). This basin is now completely inverted, overthrusting to the north the Aquitaine basin along the North Pyrenean Frontal thrust, and to the south along the Lakora thrust (figure 1).

The North Pyrenean Zone in the studied Chaînons Béarnais area contains thick and relatively complete Jurassic and Cretaceous successions and is internally deformed into a system of folds and thrusts detached in the Triassic Keuper facies (Lagabrielle et al., 2010). The Lakora thrust crops out as a gently-dipping fault, largely parallel to bedding in the upper Cretaceous cover of the Axial Zone (the footwall), and carrying a thin thrust sheet of Paleozoic, Triassic and middle-upper Cretaceous rocks in its hanging wall (Lakora klippe and Iguntze-Mendibelza massifs, figure 1; Teixell, 1990, 1996). Eastward, the Lakora thrust passes laterally to various thrusts also carrying thin Paleozoic basement slices located at the southern edge of the Chaînons Béarnais (e.g. Eaux-Chaudes and Cinq-Monts thrusts; Ternet et al., 2004). The Lakora thrust and these eastern extensions derive from the inversion of extensional structures in the upper Iberian continental margin (Teixell et al., this volume).

The southern part of the west-central Pyrenees is characterized by south-directed thrusting and includes (1) the Axial Zone, a basement antiformal culmination caused by the Gavarnie thrust, and (2) the Paleogene Jaca basin, a large-scale asymmetric synform between the Axial Zone and the South Pyrenean Frontal thrust (figure 1). Paleozoic rocks of the Axial Zone are unconformably covered by Upper Cretaceous shelf carbonates. A branch of the Lakora thrust, the Larra thrust, propagated across Upper Cretaceous-Eocene rocks of the Axial Zone cover and the northern Jaca basin. East of the study area, the Axial Zone comprises stacked basement thrust sheets that caused a greater structural relief and a large basement exposure (e.g. Roure et al., 1989; Muñoz et al., 1992). There, the northern boundary of the Axial Zone is marked by the North Pyrenean Fault, a steeply-dipping structure with complex kinematics which passes westward to a south-directed décollement at the southern edge of the Chaînons Béarnais. The westward plunge of the Axial Zone in the study area provides a constraint on the structural relief and shape of the Axial Zone top and the relationships between the main structural units. Non-exposed basement thrusts underlie the Jaca basin and cause major variations of structural relief (e.g. the Guarga thrust, figure 1b; Cámara and Klimowitz, 1985; Labaume et al., 1985; Teixell and García-Sansegundo, 1995; Teixell, 1996).

Pre-orogenic Mesozoic successions in the Jaca basin are relatively thin and incomplete; in contrast, the Paleogene infill is very thick (up to 9 km) and conforms to a typical flysch-to-molasse foreland basin sequence (Puigdefàbregas, 1975; Mutti et al., 1998). Tectonics-sedimentation relationships indicate a piggy-back sequence of thrusting from the Lakora to the Guarga thrusts which spans the entire Pyrenean orogeny. The Lakora thrust probably initiated in the late Santonian, as indicated by flexure in its footwall sediments, and its main activity continued until the middle Eocene (Bartonian). This includes the footwall splays of the Larra thrust and the laterally equivalent Eaux-Chaudes thrust (Teixell, 1996). The Gavarnie thrust was active from the late Eocene to the early Oligocene, whereas the Guarga thrust took up final compressive deformation from the late Oligocene to the earliest Miocene (Teixell, 1996).

The chronology of the North Pyrenean thrusts is less known. The internal structures of the Chaînons Béarnais were initiated during the late Jurassic - early Cretaceous as diapiric salt walls in extensional context (Canérot, 1985; Teixell et al. this volume), but their evolution in the Pyrenean orogeny is less constrained in time. The North Pyrenean Frontal thrust appears as a long-lived structure partly contemporaneous to the Lakora thrust and extending until more recent times. Indeed, in the study area, growth strata in its footwall syncline indicate thrusting beginning in Campanian-Maastrichtian times and continuing during the Paleogene (Poitevin et al., 2014), and thermochronologically-constrained cooling in the Mauléon segment of the North Pyrenean Zone, to the west of the study area, begun some 50 Ma ago (Vacherat et al., 2014). In spite of this early thrusting activity, the molasse deposition in the Aquitaine basin derived from the Pyrenean reliefs spans from the late-middle Eocene to the Miocene (Biteau et al., 2006).

The extent to which the described sequence of thrusts is reflected in exhumation history is not known yet. Northeast of the Jaca basin, AFT in the granites of the Axial Zone, yield Cenozoic cooling ages (e.g. Néouvielle and Bielsa massifs; Jolivet et al., 2007), but the degree of post-variscan reset and the amount of exhumation of the westernmost Axial Zone and the Lakora thrust are unknown. In spite of the rich tectonostratigraphic record of the Jaca basin, discrepancies remain for the timing of some major structures. Muñoz et al. (2013) recently attributed the emplacement of the Gavarnie thrust sheet to the middle Eocene, on the basis of a correlation between the basement thrust and the growing and rotating cover structures in the Aínsa basin. The previous attribution of the Gavarnie thrust to more recent times was based on the refolding it produced in the overlying Larra-Monte Perdido thrust, which was linked to the Boltaña anticline in turn dated as late Lutetian to Bartonian (Teixell, 1996).

A late Eocene to Oligocene age for the Gavarnie thrust has also been favored by Jolivet et al. (2007) on the basis of AFT ages of ca. 35 Ma of the thrust hanging wall at high elevation in the Néouvielle granite. On the other hand, AFT ages around 20 Ma dominate the southernmost Axial Zone in the central Pyrenees, in the footwall of the Gavarnie thrust (Fitzgerald et al., 1999; Sinclair et al., 2005; Jolivet et al., 2007). In post-tectonic times, an acceleration of exhumation rates at 9 Ma was detected by AHe modeling in the eastern part of the South Pyrenean foreland basin (Fillon and Van Der Beek, 2012). To date, this event has not been reported in the Axial Zone except for a 10.9 ± 1.0 Ma sample obtained by Jolivet et al. (2007) in the Bielsa massif.

3. Sampling and methods

A total of 18 samples were collected for ZHe, AFT and AHe studies and 5 more samples from Meresse (2010) were used to complete de dataset (see location in figure 2).

Five samples were taken in the Paleozoic granites of the Balaitous-Panticosa and Eaux-Chaudes plutons, and 3 in Paleozoic detrital rocks to the west to unravel the timing of exhumation of the western Axial Zone. This was complemented with the 5 previous AFT results from Meresse (2010) and new He data made on this samples. To gain insight into the activity of Lakora thrust, 2 samples were taken in Upper Cretaceous and lower Eocene turbiditic sediments from the footwall (Axial Zone cover) and 3 in Albian conglomerates from the hangingwall. To complete the study to the north, 4 samples were taken in the Chaînons Béarnais (NPZ) and 2 in the Aquitaine basin, in the footwall of the North Pyrenean Frontal Thrust.

The 9 samples that contained a sufficient number of high-quality apatites were analyzed for fission tracks and/or (U-Th)/He (tables 1 and 2). Zircon grains could be retrieved from most samples, and ZHe analyses were performed on 18 samples (table 3). Sample JA2 did not provide zircon suitable for analysis. The data obtained allowed thermal modeling of 4 profiles in the granitic massifs of Balaitous-Panticosa and Eaux-Chaudes and in the Lakora thrust sheet.

The AFT analyses were performed following the procedure described by Jolivet et al. (2007). The mounted samples were sent to Oregon State University for irradiation. Ages were calculated using an overall zeta value of 344 ± 2 a cm^2 (GVB) obtained on both Durango (McDowell et al., 2005) and Mount Dromedary (Green, 1985; Tagami, 1987) apatite standards.

Apatite (U-Th)/He dating was performed at Geosciences Montpellier, following the procedure described in Romagny et al. (2014). Prismatic apatites were selected, with 2 or nor pyramids and size ranging from 50 to 200 µm. For the samples from the Balaitous-Panticosa pluton, 2 to 3 apatite grains of the same size were used for each aliquot with the exception of sample GPY15 for which single crystals were dated. In the Eaux-Chaudes pluton, only 2 aliquots from sample GPY09 contained 2 grains.

Zircon (U-Th)/He dating was carried out at the University of Texas-Austin using laboratory procedures described in Wolfe and Stockli (2010). Individual ages were calculated using standard α-ejection corrections (e.g. Farley et al., 1996; Farley, 2002) and reported age uncertainties of about 8% (2σ) are based on the reproducibility of replicate analysis of laboratory standards (Farley et al., 2001; Reiners, 2005). Both uncorrected and α-ejection corrected ages are reported (Table 3).

4. Results

In what follows, data are organized according to the structural position of the samples in the different tectonic or lithologic units (figure 2). For ZHe ages, we present age-elevation plots and ages versus Ue plots in Annex 1 (online supplementary material).

4.1. The Chaînons Béarnais and Aquitaine Basin

The sample set of the Chaînons Béarnais and Aquitaine Basin consist of terrigenous rocks from Carboniferous to Cretaceous age which provided only zircon crystals suitable for analysis. In the Aquitaine Basin, samples ASS1 and NAY2 come from Campanian and Maastrichtian, respectively, poorly cemented sandstones and yield a dispersion of ZHe ages older than the depositional age, ranging between ~150-270 Ma (see table 3 for error margins), indicating no reset after deposition. In the Chaînons Béarnais, ZHe ages range between 26 and 50 Ma, younger than the depositional ages, and attest for exhumation in the hanging wall of the North Pyrenean Frontal thrust. Sample CTH1 yields the oldest age range (41-50 Ma) in accordance with its highest structural position in an Albian-Cenomanian syncline. The southernmost sample GPY17 from Carboniferous sandstone of the Chaînons Béarnais basement yield the younger age range between 26 and 29 Ma, in spite of a higher elevation. Samples from the Permian-Triassic red beds (LBT2 and MCT7) yield intermediate ages between 33 and 42 Ma.

4.2. *The Lakora thrust sheet*

Three samples from the Albian Mendibelza conglomerate (Boirie and Souquet, 1982) provided zircons suitable for analysis, but no apatites. The 3 samples provide ZHe ages in the late Eocene-early Oligocene interval, ranging from 27-29 Ma at the lower altitude (312 m, GPY03) to 30-35 Ma at higher altitude (1800 m in the Lakora klippe, GPY04).

4.3. *The Axial Zone cover*

In the post-variscan cover of the Axial Zone (hanging wall of the Gavarnie thrust), a Maastrichtian turbiditic sandstone (GPY07, 1579 m) provides ZHe ages of 31-36 Ma, younger than the depositional age and strikingly similar to the age in the Lakora thrust sheet just above (figure 2). A sample of lower Eocene flysch located ~5 Km to the south (GPY08, 1810 m), yields a wide dispersion of ZHe ages (37-80 Ma), some older than the depositional age, indicative of partial reset.

4.4. *The western Axial Zone: detrital Paleozoic rocks*

Samples from the westernmost Paleozoic exposures of the Axial Zone also belong to the hanging wall of the Gavarnie thrust and comprise Carboniferous and Permian sandstones that provided apatite and zircon crystals with large age dispersion. Samples JA2 and JA3 of the southern Axial Zone near the Somport pass yield comparable AFT (Meresse, 2010) and ZHe central ages which may indicate rapid cooling at 25-30 Ma, as do some zircon crystals from samples GPY05 and GPY06 from the upper Aragón Subordán valley. The latter samples show however a greater dispersion, as does a Carboniferous sandstone from the Lescun area further north (GPY14), which has a dispersion between 14 and 52 Ma (figure 2 and table 3).

4.5. *The western Axial Zone: The Eaux-Chaudes and Balaitous-Panticosa plutons*

These granitic bodies provided apatite and zircon crystals that were suitable for AFT, AHe and ZHe analysis. Most of the samples show ZHe ages independent of the eU concentration, suggesting complete reset (see Annex 1). In the Eaux-Chaudes pluton, samples GPY11 and GPY12 yield similar ZHe and AFT ages which may be indicative of rapid cooling between 20 and 25 Ma, further attested by the similarity in age between the samples in spite of a difference in elevation of 531 m. Sample GPY09 at an intermediate altitude yields a ZHe age of 24-28 Ma, while the AFT age is significantly younger, around 12 Ma (figures 2 and 3, tables 1 and 3). In the Balaitous-Panticosa granites, ZHe ages are also markedly clustered at 20-25 Ma for different elevations. However, samples BA1 and BA5 from the Balaitous mountain give AFT ages of 28-29 Ma (Meresse, 2010), slightly older than the ZHe ages obtained for the same samples in this study (table 3). Sample GPY15 at lower elevation yields an AFT age of 18 Ma, whereas ZHe ages are more dispersed (18-36 Ma). The AHe ages obtained for this set of samples range between 21 and 6 Ma with a cluster between 6 and 10 Ma, again younger than the AFT ages (table 2, figure 3) but with similar age if we take into account the 2σ errors of both AFT and AHe data.

5. Thermal modeling

Thermal history modeling was performed using QTQt software (Gallagher et al., 2009; Gallagher, 2012). For AFT modeling of the only sample with confined track lengths (GPY11) we used Ketcham et al.'s (2007) multikinetic annealing model, with the D_{par}

parameter as kinetic constrain. (U-Th)/He ages were modeled using a spherical diffusion domain (based on crystal's equivalent spherical radius), and taking into account eU-dependent radiation damage modulated diffusivity for He diffusion, following the models of Flowers et al. (2009) and Guenthner et al. (2013). In cases where AHe ages were obtained by multigrain aliquots we did not use a specific diffusion model. Models were run for the sub-vertical profiles at the Balaitous-Panticosa and Eaux-Chaudes granites and at the Lakora thrust sheet. All models were forced to be at surface temperature at present time and we allowed the temperature offset between samples to vary through time in a range equivalent to geothermal gradients of 15 to 35°C/km.

For the Balaitous-Panticosa and Eaux-Chaudes granites, independent constraints derived from field geology (unconformity of the Cenomanian carbonates above Paleozoic rocks of the Axial Zone), were used as input parameters in the thermal models to force the cooling curves to pass near the surface in Cenomanian times. The profile in the hangingwall of the Lakora thrust was constrained to pass near the surface in Albian times (stratigraphic age of the Mendibelza conglomerate), whereas a model of the westernmost Axial Zone (Paleozoic rocks and their cover) was constrained to be at shallow levels from the Cenomanian to the early Eocene.

Models of the Eaux-Chaudes and Balaitous-Panticosa sub-vertical profiles show similar results with a fast exhumation from ~30 Ma to ~20 Ma (figure 4). Prior to that age interval, the thermal history is not well constrained by the data as reflected by the high degree of uncertainty in the thermal path, taking into account the 95% credible intervals (figure 4A and 4B). After 20 Ma, the Eaux-Chaudes profile shows a slower cooling towards the surface. In contrast, the Balaitous-Panticosa profile shows a period of stability, although not well constrained by the data, with a last rapid cooling event at 8-9 Ma. The mean geothermal gradient inferred from the temperature offset between samples is of 25°C/km with no major variation over time (figure 4C and 4D). ZHe and AHe ages predicted from modeling are coherent within error margins with the observed ages. AFT show worse predicted ages; therefore, the predicted ages are within the error margins of the observed AFT ages only in the case of GPY09 and GPY15 (figures 4E and 4F).

Modeling results of the Lakora thrust sheet show that the samples crossed the lower limit of the zircon partial-retention zone (ZPRZ) at 50-42 Ma (bottom and top samples) with a moderate rate of cooling, and passed through the upper limit of the ZPRZ at 25-30Ma (figure 5). The pre-Eocene thermal history is not well constrained due to large uncertainties in the models, reflected by the 95% credible intervals (figure 5A). Therefore, the onset age of exhumation cannot be determined from the models, although modeling suggests they were already exhuming by 50-42 Ma. Above the ZPRZ the thermal path is not constrained as no AFT and AHe ages were obtained in those samples. As shown in figure 5E the model-predicted ages are consistent, within error margins, with the observed ages.

The modeled thermal path of the Lakora thrust's footwall indicates a fast cooling at ~25 Ma, followed by a slower rate final cooling from 25 Ma to Present. However, this final cooling pattern is not well constrained since AHe ages were only obtained from one sample (figure 5B). Data modeling shows a constant geothermal gradient of 25ºC/km, inferred from the offset between samples. In this case, ZHe ages are badly predicted as shown in figure 5F. Samples from this vertical profile show large intra-sample age dispersion that cannot be predicted by the QTQt software, indicating that the dispersion cannot be explained by crystals eU content or size. The age dispersion could be produced, for example, by complex internal zonation in zircon grains, which are not incorporated in the modeling due to lack of information. The poor predictions showed by the model imply that this last cooling history should be considered with caution.

6. Interpretation and discussion

Single-grain dating performed in this study provide the following five main results: (1) In the Aquitaine basin, ZHe data indicate no post-depositional reset of ages, (2) The Chaînons Béarnais of the North Pyrenean Zone record a protracted exhumation between 50 and 26 Ma (Eocene to Oligocene), (3) The Lakora thrust sheet was exhumed through the ZHe closure temperature together with its footwall (upper levels of the Gavarnie thrust sheet) at 30-36 Ma (late Eocene to Oligocene), (4) The granitic massifs of Eaux-Chaudes and Balaitous-Panticosa, and the upper Paleozoic rocks of the Somport area, all located in the Gavarnie thrust sheet, record a rapid exhumation at 26-20 Ma (late Oligocene to Aquitanian), and (5) The granitic massifs record a final acceleration of exhumation at 8-9 Ma (late Miocene) that is constrained by the AHe data. Thermal models further constrain the cooling history of the Lakora thrust sheet indicating it was exhuming at least between 50-42 Ma and 30-25 Ma (early Eocene to Oligocene), and better define the rapid exhumation history of the Eaux-Chaudes and Balaitous-Panticosa granites.

In what follows we interpret the obtained cooling ages and paths as indicating exhumation primarily linked to the activity of tectonic units, although we understand that climatic events may have played a role to an unknown degree. The samples from the uppermost Cretaceous rocks of the Aquitaine basin preserve ZHe detrital ages older than the stratigraphic age indicating that burial under Cenozoic foreland basin deposits was not enough to reset the ZHe system. This is consistent with the limited degree of diagenesis and cementation observed in these rocks. This pattern changes across the NPFT, where rocks from Paleozoic to Albian age have been buried and heated enough to reset the ZHe system. In the Chaînons Béarnais area, the effect of burial was reinforced by high heat flow during the middle and late Cretaceous times, detected by Raman spectroscopy of carbonaceous material that provided paleo-temperatures of 250-300°C (Clerc et al., 2015). The range of ZHe cooling ages obtained attest for long-lived exhumation in the North Pyrenean Zone initiating at ~50 Ma (including the Lakora thrust hanging wall), consistent with thermal modeling by Vacherat et al. (2014) in the Mauléon basin. To the east of the study area, AFT ages by Meresse (2010) from the Bagnères de Bigorre North-Pyrenean massif were centered at ca. 41 Ma. Farther east, along the ECORS-Pyrénées transect, most of the AFT data from the North-Pyrenean basement rocks indicate exhumation during the Eocene (Morris et al., 1998; Fitzgerald et al., 1999). These data together support an early exhumation of the North-Pyrenean Zone during the early to middle Eocene. In the study area, we associate the exhumation of the Chaînons Béarnais to the pop-up extrusion of the former North Pyrenean basin by the NPFT to the north and the Lakora thrust and its eastern extensions such as the Eaux-Chaudes thrust (Teixell et al., this volume). Younger cooling ages obtained in the area, especially at deep stratigraphic levels, indicate that thrust-related exhumation proceeded during younger times, caused by continued uplift on the NPFT and probably also by the thick-skinned basement thrusts of the southern Pyrenees, such as the Gavarnie and Guarga thrusts (figure 1b). ZHe ages centered on 34-40 Ma in Permian-Triassic rocks indicate exhumation during middle and late Eocene to Oligocene consistent with the onset of molasse sedimentation of this age in the Aquitaine basin (Biteau et al., 2006). On the other hand, the southward extent of the Lakora thrust sheet is constrained by the non-completely reset Eocene sample from Pico Matz (GPY08), in agreement with the hangingwall ramp of Lakora thrust observed in the Lakora klippe 6 km to the north of Pico Matz.

ZHe ages indicate that the Lakora thrust sheet and its immediate footwall of the Axial Zone cover underwent joint exhumation at 30-36 Ma (late Eocene to Oligocene), which we must attribute to thrust faulting under the Axial Zone. This cooling age is correlative with late Eocene to early Oligocene conglomerate pulses in the Jaca basin, which are dominated by clasts derived from lower to middle Eocene turbidites (Puigdefàbregas, 1975; Roigé et al., this volume). We attribute this event to the motion along the Gavarnie thrust (figure 1b), because it is the first major south-directed thrust that underlies the Axial Zone in the study area, producing a significant duplication of Paleozoic rocks and creating a marked structural relief. This interpretation is in agreement with the timing of the Gavarnie thrust proposed by Teixell (1996), Jolivet et al., (2007) and Labaume et al. (in rev.) on the basis of structural relationships and tectonics-sedimentation relationships in the Jaca basin, and differs from Muñoz et al. (2013) attribution of the thrust to the middle Eocene. It could be argued that the entire profile of the Gavarnie thrust sheet was emplaced below the ZPRZ, and that all the exhumation was driven by the underlying Guarga thrust (figure 1b), from the late Eocene to the Miocene (e.g. samples from Balaitous, Panticosa and Eaux-Chaudes). We consider this unlikely for the study area on the basis of fault slip magnitudes and cross-section balancing in the Jaca basin (e.g. Teixell, 1996), even if the Guarga thrust causes a component of uplift on the Axial Zone. No distinct thermochronology signal can be attributed to the Larra thrust, probably because this thin-skinned branch of the Lakora thrust did not create significant structural relief during its propagation in the Jaca basin fill during the Lutetian-Bartonian.

Following these considerations, we attribute the second ZHe age cluster at 20-26 Ma observed in the western Axial Zone and the fast cooling between 30 and 20 Ma modeled in the granitic massifs to the east to continued uplift of the Axial Zone along the Guarga thrust. This activity of the Guarga thrust was correlated to the main emergence of the South Pyrenean thrust front of the External Sierras, recorded by the late Oligocene to Aquitanian conglomerates and fluvial sandstones of the Uncastillo Formation (Puigdefàbregas, 1975; Teixell, 1996; Millán et al., 2000).

AHe data show exhumation signals between 6 and 10 Ma in the Eaux-Chaudes and Balaitous-Panticosa plutons, with samples located on both sides of the present drainage divide (figure 2). In the Balaitous-Panticosa profile, samples on both sides of the divide can be fit in a single coherent model, indicating that they experienced a similar cooling history. Therefore, the incision during this time could not be caused by the capture of the south-flowing Ebro river as defended by Fillon and Van Der Beek (2012).

7. Conclusions

A low-temperature thermochronology study of the western Axial Zone of the Pyrenees and of the adjacent Chaînons Béarnais (North Pyrenean Zone) provides the following constraints on the tectonic and erosional history of this segment of the chain:

- The uppermost Cretaceous foreland basin sediments of the Aquitaine basin have not been buried enough for post-depositional reset of the ZHe thermochronology system and preserve Permian to Jurassic detrital signals.
- Within the Chaînons Béarnais, the ZHe system was reset and record continued pop-up like exhumation of the North Pyrenean Zone between the North Pyrenean Frontal Thrust and the major south-directed thrusts of Lakora and others further south (Gavarnie and Guarga) from 50 to 26 Ma (Eocene to Oligocene).
- The leading edge of the Lakora thrust sheet, which was reported to bring the North Pyrenean Zone on top of the Axial Zone during late Cretaceous to middle Eocene times, shows a cooling path at least from early Eocene to Oligocene times. The Lakora thrust sheet together with its immediate footwall forming the post-variscan cover of the Axial Zone were exhumed through the ZHe closure temperature at 36-30 Ma (late Eocene to Oligocene) along the underlying Gavarnie thrust. Hence, the cooling path of the Lakora

thrust sheet is the result of the activity of the Lakora thrust itself and of the underlying Gavarnie (and possibly Guarga) thrusts.

- Paleozoic sediments of the westernmost Axial Zone often yield scattered ZHe thermochronology results indicating partial reset. The granite samples from the Eaux-Chaudes and Balaitous-Panticosa plutons provide a good ZHe and AFT late Paleogene to Miocene signal, clearly reflected in models as fast cooling between 30 and 20 Ma (late Oligocene to Aquitanian). We attribute this cooling to thrusting on the Guarga thrust, ultimately uplifting the older Gavarnie thrust sheet lying above.
- AHe results from the Eaux-Chaudes and Balaitous-Panticosa plutons cluster at 9-8 Ma (late Miocene) attesting for post-orogenic cooling that was detected in previous studies of the southern foreland basin.

Acknowledgements

This work was supported by projects CGL2010-15416 and CGL2014-54180-P (MINECO, Spain) and PYRAMID (ANR, France), and by Géosciences Montpellier. We acknowledge the constructive reviews by Luis Barbero, Camille Clerc and Yves Lagabrielle which helped to improve the manuscript. Andreu Badia is thanked for field assistance during sampling.

References

Barnolas, A., Teixell, A., 1994. Platform sedimentation and collapse in a carbonate-dominated margin of a foreland basin (Jaca basin, Eocene, southern Pyrenees). Geology 22, 1107-1110.

Beamud, E., Muñoz, J.A., Fitzgerald, P.G., Baldwin, S.L., Garcés, M., Cabrera, L., Metcalf, J.R., 2011. Magnetostratigraphy and detrital apatite fission track thermochronology in syntectonic conglomerates: constraints on the exhumation of the South-Central Pyrenees. Basin Res. 23, 309-331.

Biteau, J.-J., Le Marrec, A., Le Vot, M., Masset, J.-M., 2006. The Aquitaine Basin. Petroleum Geoscience 12, 247-273.

Boirie, J.M., Souquet, P., 1982. Les poudingues de Mendibelza: dépots de cônes sous-marins du rift albien des Pyréneés. Bull. Centr. Rech. Explor.-Prod. Elf Aquitaine 6, 405-435.

Cámara, P., Klimowitz, J., 1985. Interpretacion geodinámica de la vertiente centro-occidental surpirenaica. Estudios geologicos 41, 391-404.

Clerc, C., Lahfid, A., Monié, P., Lagabrielle, Y., Chopin, C., Poujol, M., Boulvais, P., Ringenbach, J.-C., Masini, E., de St Blanquat, M., 2015. High-temperature metamorphism during extreme thinning of the continental crust: a reappraisal of the North Pyrenean passive paleomargin. Solid Earth 6, 643–668.

Farley, K.A., 2002. (U–Th)/He dating: techniques, calibrations, and applications. In: Porcelli, D., Ballentine, C.J.,Wieler, R. (Eds.), Noble gases in geochemistry and cosmochemistry. Rev. Miner. 47, 819–844.

Farley, K.A., Wolf, R., Silver, L., 1996. The effects of long alpha-stopping distances on (U-Th)/He ages. Geochim. Cosmochim. Acta 60, 4223-4229.

Farley, K.A., Rusmore, M.E., Bogue, S.W., 2001. Post-10 Ma uplift and exhumation of the northern coast mountains, British Columbia. Geology 29, 99-102.

Fillon, C., Van Der Beek, P., 2012. Post-orogenic evolution of the southern Pyrenees: constraints from inverse thermo-kinematic modelling of low-temperature thermochronology data. Basin Res. 24, 418–436.

Fitzgerald, P.G., Muñoz, J.A., Coney, P.J., Baldwin, S.L., 1999. Asymmetric exhumation across the Pyrenean orogen: implications for the tectonic evolution of a collisional orogen. Earth Planet. Sci. Lett. 173, 157–170.

Flowers, R. M., Ketcham, R.A., Shuster, D. L., Farley, K. A., 2009. Apatite (U–Th)/He thermochronometry using a radiation damage accumulation and annealing model. Geochim. Cosmochim. Acta 73, 2347–2365.

Gallagher, K., 2012. Transdimensional inverse thermal history modelling for quantitative thermochronology, J. Geophys. Res. 117, B02408, doi:10.1029/2011JB00882.

Gallagher, K., Charvin, K., Nielsen, S., Sambridge, M., Stephenson, J., 2009. Markov chain Monte Carlo (MCMC) sampling methods to determine optimal models, model resolution and model choice for Earth Science problems. Mar. Petrol. Geol. 26, 525-535.

Gibson, M., Sinclair, H.D., Lynn, G.J., Stuart, F.M., 2007. Late- to post-orogenic exhumation of the Central Pyrenees revealed through combined thermochronological data and modeling. Basin Res. 19, 323-334.

Green, P.F., 1985. A comparison of zeta calibration baselines in zircon, sphene and apatite. Chem. Geol., 58, 1-22.

Guenthner, W.R., Reiners, P.W., Ketcham, R.A., Nasdala, L., Giester, G., 2013. Helium diffusion in natural zircon: Radiation damage, anisotropy, and the interpretation of zircon (U-Th)/He thermochronology. Amer. J. Sci. 313, 145–198.

Gunnell, Y., Calvet, M., Brichau, S., Carter, A., Aguilar, J.-P., Zeyen, H., 2009. Low long-term erosion rates in high-energy mountain belts: Insights from thermo- and biochronology in the Eastern Pyrenees. Earth Planet. Sci. Lett. 278, 208–218.

Jammes, S., Manatschal, G., Lavier, L., Masini, E., 2009. Tectono-sedimentary evolution related to extreme crustal thinning ahead of a propagating ocean: the example of the western Pyrenees. Tectonics 28, TC4012, doi:10.1029/2008TC002406.

Jolivet, M., Labaume, P., Monié, P., Brunel, M., Arnaud, N., Campani, M., 2007. Thermochronology constraints for the propagation sequence of the south-Pyrenean basement thrust system (France-Spain). Tectonics 26, doi:10.1029/2006TC002080.

Ketcham, R.A., Carter, A., Donelick, R.A., Barbarand,J., Hurford, A.J., 2007. Improved modelling of fission-track annealing in apatite. American Mineralogist, 92, 789-798.

Labaume, P., Séguret, M., Seyve, C., 1985. Evolution of a turbiditic foreland basin and analogy with an accretionary prism: Example of the Eocene South-Pyrenean basin. Tectonics 4, 661-685.

Lagabrielle, Y., Bodinier, J.L., 2008. Submarine reworking of exhumed subcontinental mantle 348 rocks: field evidence from the Lherz peridotites, French Pyrenees. Terra Nova, 20, 11-21.

Labaume, P., Meresse, P., Jolivet, M., Teixell, A., Lahfid, A. Tectono-thermal history of an exhumed thrust-sheet-top basin: an example from the south Pyrenean thrust belt. Tectonics, In review.

Maurel, O., Monié, P., Pik, R., Arnaud, N., Brunel, M., Jolivet, M., 2007. The Meso-Cenozoic thermo-tectonic evolution of the Eastern Pyrenees: an 40Ar/39Ar fission track and (U–Th)/He thermochronological study of the Canigou and Mont-Louis massifs. Int. J. Earth Sci. 97, 565–584.

McDowell, F.W., McIntosh, W.C., Farley, K.A., 2005. A precise 40Ar-39Ar reference age for the Durango apatite (U-Th)/He and fission-track dating standard. Chem. Geol., 214, 249-263.

Meresse, F., 2010. Dynamique d'un prisme orogénique intracontinental: évolution thermochronologique (traces de fission sur apatite) et tectonique de la Zone Axiale et des piedmonts des Pyrénées centro-occidentales. Thèse Doct., Université de Montpellier II, Montpellier, France, 277 p.

Metcalf, J.R., Fitzgerald, P.G., Baldwin, S.L., Muñoz, J.-A., 2009. Thermochronology of a convergent orogen: Constraints on the timing of thrust faulting and subsequent exhumation of the Maladeta Pluton in the Central Pyrenean Axial Zone. Earth Planet. Sci. Lett. 287, 488–503.

Millán, H., Pueyo, E. L., Aurell, M., Aguado, A., Oliva, B., Martínez Peña, M. B., Pocoví, A., 2000. Actividad tectónica registrada en los depósitos terciarios del frente meridional del Pirineo central. Rev. Soc. Geol. España 13, 279-300.

Morris, R.G., Sinclair, H.D., Yelland, A.J., 1998. Exhumation of the Pyrenean orogen: implications for sediment discharge. Basin Res. 10, 69–85.

Mouthereau, F., Filleaudeau, P.-Y., Vacherat, A., Pik, R., Lacombe, O., Fellin, M.G., Castelltort, S., Christophoul, F., Masini, E., 2014.Placing limits to shortening evolution in the Pyrenees: Role of margin architecture and implications for the Iberia/Europe convergence. Tectonics 33, doi:10.1002/2014TC003663.

Muñoz, J.A., 1992., Evolution of a continental collision belt: ECORS-Pyrenees crustal balanced cross-section. In: McClay, K.R. (Ed.), Thrust Tectonics, Chapman and Hall, London, UK, pp. 235-246.

Muñoz, J.A., Beamud, E., Fernández, O., Arbués, P.,Dinarès-Turell, J., Poblet, J., 2013. The Aínsa fold and thrust oblique zone of the central Pyrenees: Kinematics of a curved contractional system from paleomagnetic and structural data. Tectonics 32, 1142-1175.

Mutti, E., Séguret, M., Sgavetti, M., 1988. Sedimentation and deformation in the Tertiary sequences of the southern Pyrenees. Field Trip Guidebook 7, AAPG Mediterranean Basins Conference, Nice, 169 p.

Poitevin, C., Labaume, P., Gay, A., Teixell, A., 2014. Du rifting à l'inversion pyrénéenne dans le Bassin d'Aquitaine : interprétation du profil sismique St-Pé de Bigorre-Condom. Rés. 24e Réunion des Sciences de la Terre, Pau, p. 327.

Puigdefàbregas, C., 1975. La sedimentación molásica en la cuenca de Jaca. Pirineos 104, 1-188.

Reiners, P.W., Spell, T.L., Nicolescu, S., Zanetti, K.A., 2004. Zircon (U-Th)/He thermochronometry: He diffusion and comparisons with 40Ar/39Ar dating. Geochim. Cosmochim. Acta 68, 1857–1887.

Roigé, M., Gómez-Gras, D., Remacha, E., Daza, R., Boya, S., Provenance of the clastic systems of the Jaca basin, related to the sea retreat after prevalence of deep-marine environments (Middle and Upper Eocene of the South-Central Pyrenees). C. R. Geoscience, this volume.

Romagny, A., Münch, P., Cornée, J. J., Corsini, M., Azdimousa, A., Melinte-Dobrinescu, M. C., Drinia, H., Bonno, M., Arnaud, N., Monié, P., Quillévéré, F., Ben Moussa, A., 2014. Late Miocene to present-day exhumation and uplift of the Internal Zone of the Rif chain: Insights from low temperature thermochronometry and basin analysis. J. Geodyn. 77, 39-55.

Roure, F., Choukroune, P., Berástegui, X., Muñoz, J.A., Villien, P., Matheron, P., Bareyt, M., Séguret, M., Camara, P., Déramond, J., 1989. ECORS Deep Seismic data and data and balanced cross-sections: Geometric constraints on the evolution of the Pyrenees. Tectonics 8, 41-50.

Rushlow, C.R., Barnes, J.B., Ehlers, T.A., Vergés, J. 2013. Exhumation of the southern Pyrenean fold-thrust belt (Spain) from orogenic growth to decay. Tectonics 32, 843–860.

Sinclair, H.D., Gibson, M., Naylor, M., Morris, R.G., 2005. Asymmetric growth of the Pyrenees revealed through measurement and modeling of orogenic fluxes. Amer. J. Sci. 305, 369-406.

Tagami, T., 1987. Determination of zeta calibration constant for fission track dating. Nucl. Tracks Radiat. Meas., 13, 127-130.

Teixell, A.,1990. Alpine thrusts at the western termination of the Pyrenean Axial Zone, Bull. Soc. géol. France 8, 241-249.

Teixell, A., 1996. The Ansó transect of the southern Pyrenees: basement and cover thrust geometries. J. Geol. Soc. London 153, 301-310.

Teixell, A., 1998. Crustal structure and orogenic material budget in the west-central Pyrenees. Tectonics 17, 395-406.

Teixell, A., García-Sansegundo, J., 1995. Estructura del sector central de la Cuenca de Jaca (Pirineo central). Rev. Soc. Geol. España 8, 207-220.

Teixell, A., Muñoz, J. A., 2000. Evolución tectono-sedimentaria del Pirineo meridional durante el Terciario: una síntesis basada en la transversal del río Noguera Ribagorçana. Rev. Soc. Geol. España 13, 251–264.

Teixell, A., Labaume, P., Lagabrielle, Y., The crustal evolution of the west-central Pyrenees revisited: inferences from a new kinematic scenario. C. R. Geoscience, this volume.

Ternet, Y., Majesté-Menjoulàs, C., Canérot, J., Baudin, T., Cocherie, A., Guerrot, C., Rossi, P., 2004. Notice explicative, carte géol. France (1/50.000), feuille Laruns-

Somport (1069). Orléans : BRGM, 192 p. Carte géologique par Ternet Y., Majesté-Menjoulàs C., Canérot J., Baudin T., Cocherie A., Guerrot C., Rossi P. (2004).

Vacherat, A., Mouthereau, F., Pik, R., Bernet, M., Gautheron, C.,Masini, E., Le Pourhiet, L.,Tibaric, B.,Lahfid. A., 2014. Thermal imprint of rift-related processes in orogens as recorded in the Pyrenees. Earth Planet. Sci. Letters 408, 296-306.

Whitchurch, A.L., Carter, A., Sinclair, H.D., Duller, R.A., Whittaker, A.C., Allen, P.A., 2011. Sediment routing system evolution within a diachronously uplifting orogen: Insights from detrital zircon thermochronological analyses from the South-Central Pyrenees. Am. J. Sci. 311, 442–482.

Wolfe, M.R., Stockli, D.F., 2010. Zircon (U–Th)/He thermochronometry in the KTB drill hole, Germany, and its implications for bulk He diffusion kinetics in zircon. Earth Planet. Sci. Letters 295, 69–82.

Yelland, A.J., 1990. Fission track thermotectonics in the Pyrenean orogen. Nucl. Tracks Radiat. Meas. 17, 293-299

TABLE 1

Apatite fission track results. Nb of grains is the number of crystals analysed. ρ_d is the density of induced fission track density (per cm²) that would be obtained in each individual sample if its U concentration was equal to the U concentration of the CN5 glass dosimeter. Number in brackets is the total number of tracks counted. ρ_S and ρ_i represent sample spontaneous and induced track densities per cm². Number in brackets is the total number of tracks counted. [U] is the calculated uranium density. $P(\chi^2)$ is the probability in % of χ^2 for v degrees of freedom (where v = number of crystals – 1). D_{par} is the mean fission-track pit diameter in µm corrected following Sobel and Seward (2010) using a correction factor of 0.825. Ages have been calculated using the Trackkey software (Dunkl, 2002). Samples indicated # are from Meresse (2010).

TABLE 2

Apatite (U-Th)/He results. Nb of grains is the number of crystals analyzed into an aliquot; FT, geometric correction factor for age calculation; corrected age is the age corrected with the FT factor; the uncertainty of 1σ was fixed at 8% of the age; mean age, the pondered mean of the aliquot ages in each sample.

TABLE 3

Zircon (U-Th)/He results. FT, geometric correction factor for age calculation; eU, effective uranium concentration; corrected age, age corrected with the FT factor; the uncertainty of 1σ was fixed at 8% of the age; mean age, the pondered mean of the aliquot ages in each sample.

FIGURE CAPTIONS

Figure 1. a) Geological sketch of the Pyrenees with previous thermochronology results obtained in the Axial Zone (Morris et al., 1998; Fitzgerald et al., 1999; Sinclair et al., 2005; Gibson et al., 2007; Jolivet et al., 2007; Maurel et al., 2008; Gunnell et al., 2009; Metcalf et al., 2009). MB: Mauleon basin, LT: Lakora Thrust, ChB: Chainons Bearnais, GT: Gavarnie Thrust. b) Simplified cross-section across the west-central Pyrenees showing the main tectonic units discussed in this work and projected structural locations of the studied samples (large stars: several samples; small stars: single samples; Ansó-Arzaq transect of Teixell, 1988).

Figure 2. Map of the western Pyrenean Axial Zone and adjacent Chaînons Béarnais showing location of samples and thermochronological results; ZHe results in green, AFT in red and AHe in blue. For He data we indicate the age ranges (see tables 1, 2 and 3 for further information). The blue dashed line indicates the drainage divide.

Figure 3. AFT Age-elevation plot of the Eaux-Chaudes and Balaitous-Panticosa granodiorites dataset (in red), and of the GPY14 sample from Paleozoic sediments in the westernmost Axial Zone (black).

Figure 4. (A, B) Modeled thermal history of the Eaux-Chaudes and Balaitous-Panticosa sub-vertical profiles. The red line corresponds to the path of the hottest (lowest elevation) sample (with 95% credible interval range in magenta) and the blue line corresponds to the coolest (highest elevation) sample (with 95% credible interval range in cyan). Intermediate samples are shown in grey. Black boxes correspond to the constraints imposed on the

modeling (see text for further information). (C, D) modeled geothermal gradients in red with 95% credible interval range in grey. (E, F) Observed and model-predicted AHe and ZHe uncorrected ages versus elevation. Predicted track length distribution on sample GY11 is plotted in red with 95% credible intervals in orange in comparison with observed track length data (histograms).

Figure 5. (A, B) Modeled thermal history of the vertical profile located in the footwall and hangingwall of the Lakora thrust. The red line corresponds to the path of the hottest (lowest elevation) sample (with 95% credible interval range in magenta). The blue line corresponds to the coolest (highest elevation) sample (with 95% credible interval range in cyan). Intermediate samples are shown in grey. Black boxes correspond to the constraints imposed into the modeling (see the text for further information). (C, D) modeled geothermal gradients in black with 95% credible interval range in grey. (E, F) Observed and modeled predicted AHe and ZHe uncorrected ages versus elevation.

Figure 1

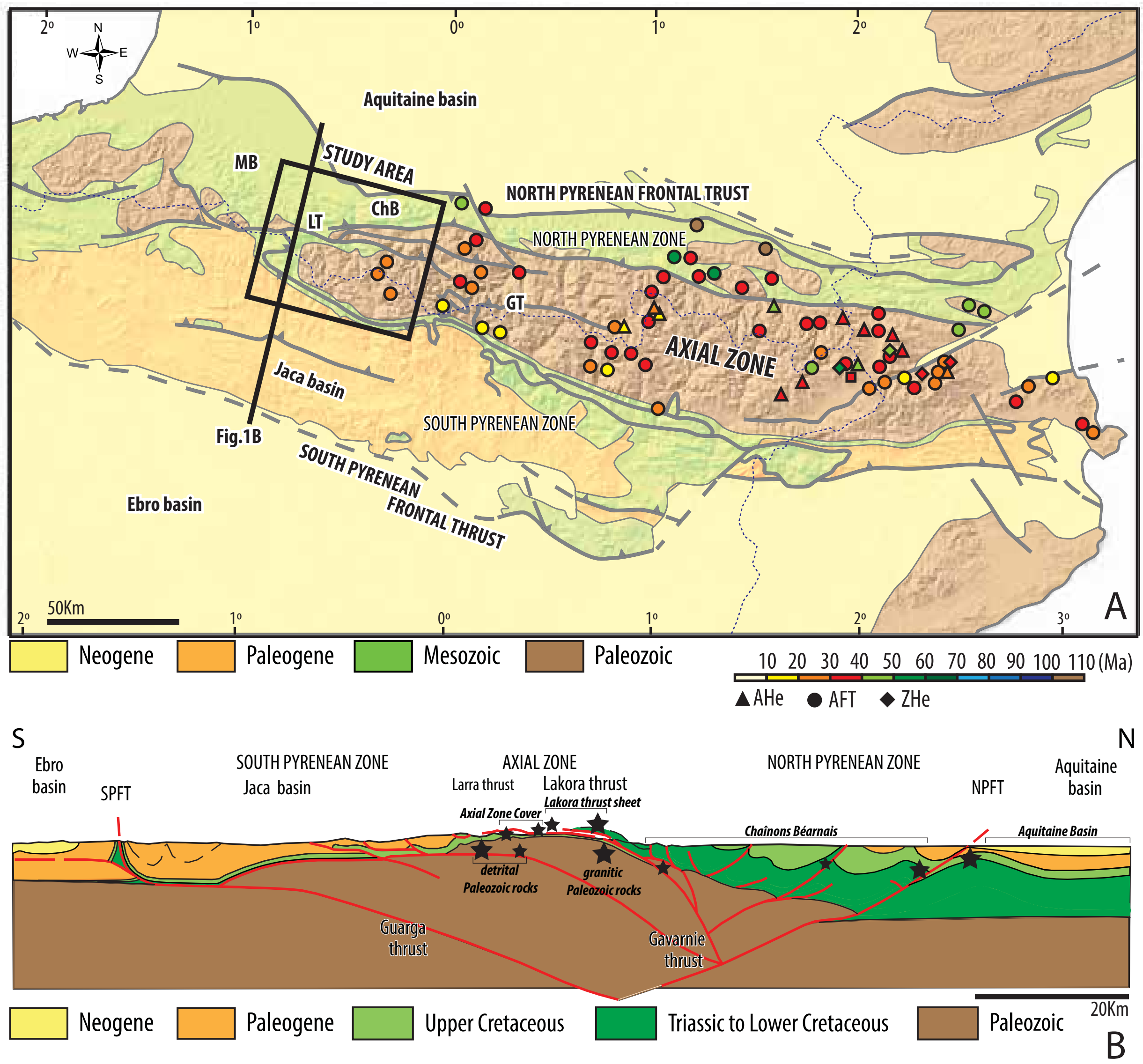

N
W
E
S
Aquitaine basin
STUDY AREA
MB
LT
ChB
NORTH PYRENEAN FRONTAL TRUST
NORTH PYRENEAN ZONE
GT
AXIAL ZONE
Jaca basin
Fig.1B
SOUTH PYRENEAN ZONE
SOUTH PYRENEAN FRONTAL THRUST
Ebro basin
50Km
A
Neogene
Paleogene
Mesozoic
Paleozoic
10 20 30 40 50 60 70 80 90 100 110 (Ma)
AHe
AFT
ZHe
S
N
Ebro basin
SPFT
SOUTH PYRENEAN ZONE
Jaca basin
AXIAL ZONE
Larra thrust
Lakora thrust
Lakora thrust sheet
Axial Zone Cover
detrital Paleozoic rocks
granitic Paleozoic rocks
NORTH PYRENEAN ZONE
Chaînons Béarnais
NPFT
Aquitaine basin
Aquitaine Basin
Guarga thrust
Gavarnie thrust
20Km
Neogene
Paleogene
Upper Cretaceous
Triassic to Lower Cretaceous
Paleozoic
B

Figure 2

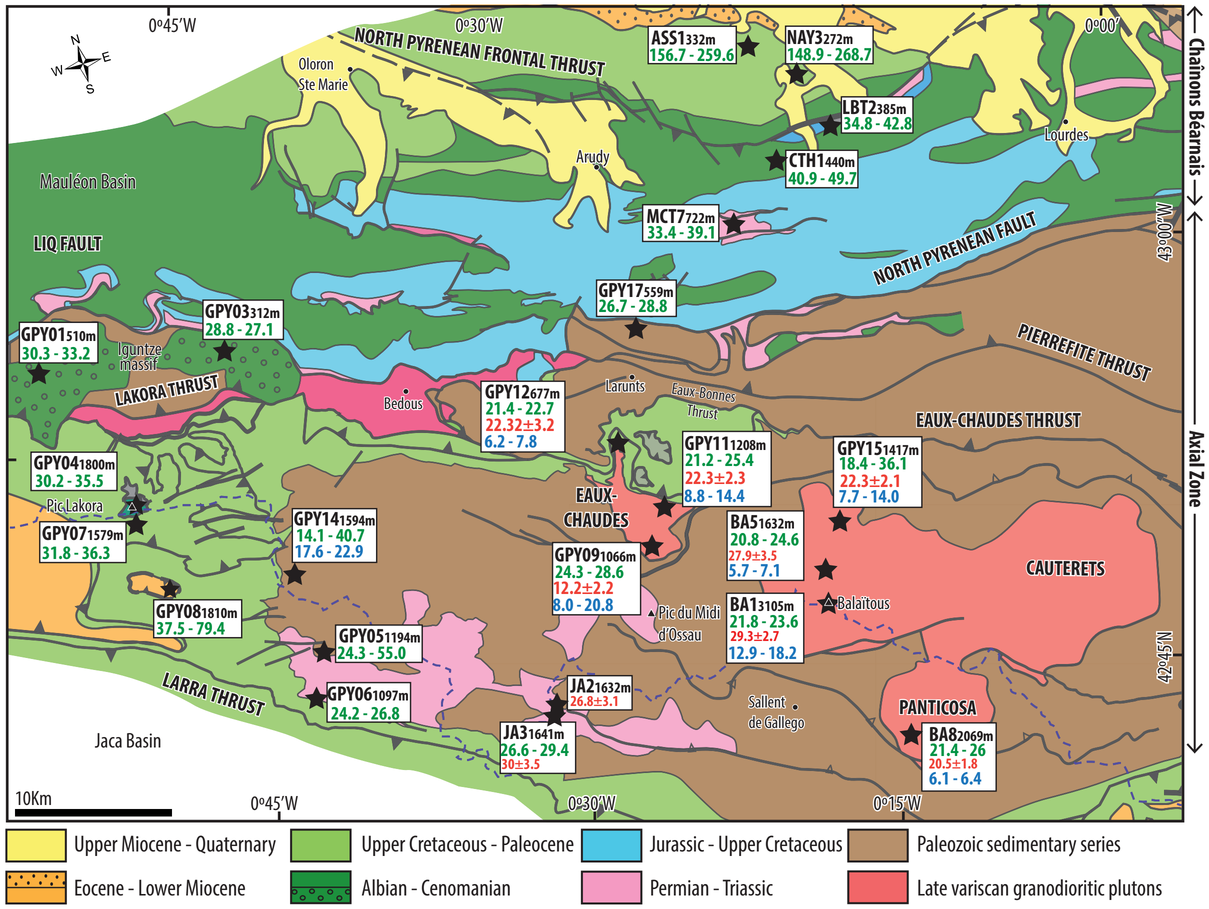

NORTH PYRENEAN FRONTAL THRUST
Oloron Ste Marie
Mauléon Basin
LIQ FAULT
Arudy
Lourdes
NORTH PYRENEAN FAULT
PIERREFITE THRUST
EAUX-CHAUDES THRUST
LAKORA THRUST
Iguntze massif
Bedous
Laruns
Eaux-Bonnes Thrust
EAUX-CHAUDES
CAUTERETS
Pic Lakora
Pic du Midi d'Ossau
Balaïtous
Sallent de Gallego
PANTICOSA
LARRA THRUST
Jaca Basin
10Km
0°45'W
0°30'W
0°15'W
0°00'
43°00'N
42°45'N
Chaînons Béarnais
Axial Zone
ASS1 332m 156.7 - 259.6
NAY3 272m 148.9 - 268.7
LBT2 385m 34.8 - 42.8
CTH1 440m 40.9 - 49.7
MCT7 722m 33.4 - 39.1
GPY17 559m 26.7 - 28.8
GPY03 312m 28.8 - 27.1
GPY01 510m 30.3 - 33.2
GPY12 677m 21.4 - 22.7 22.32±3.2 6.2 - 7.8
GPY11 1208m 21.2 - 25.4 22.3±2.3 8.8 - 14.4
GPY15 1417m 18.4 - 36.1 22.3±2.1 7.7 - 14.0
GPY04 1800m 30.2 - 35.5
GPY07 1579m 31.8 - 36.3
GPY14 1594m 14.1 - 40.7 17.6 - 22.9
BA5 1632m 20.8 - 24.6 27.9±3.5 5.7 - 7.1
GPY09 1066m 24.3 - 28.6 12.2±2.2 8.0 - 20.8
BA1 3105m 21.8 - 23.6 29.3±2.7 12.9 - 18.2
GPY08 1810m 37.5 - 79.4
GPY05 1194m 24.3 - 55.0
JA2 1632m 26.8±3.1
GPY06 1097m 24.2 - 26.8
JA3 1641m 26.6 - 29.4 30±3.5
BA8 2069m 21.4 - 26 20.5±1.8 6.1 - 6.4
Upper Miocene - Quaternary
Upper Cretaceous - Paleocene
Jurassic - Upper Cretaceous
Paleozoic sedimentary series
Eocene - Lower Miocene
Albian - Cenomanian
Permian - Triassic
Late variscan granodioritic plutons

Figure 3

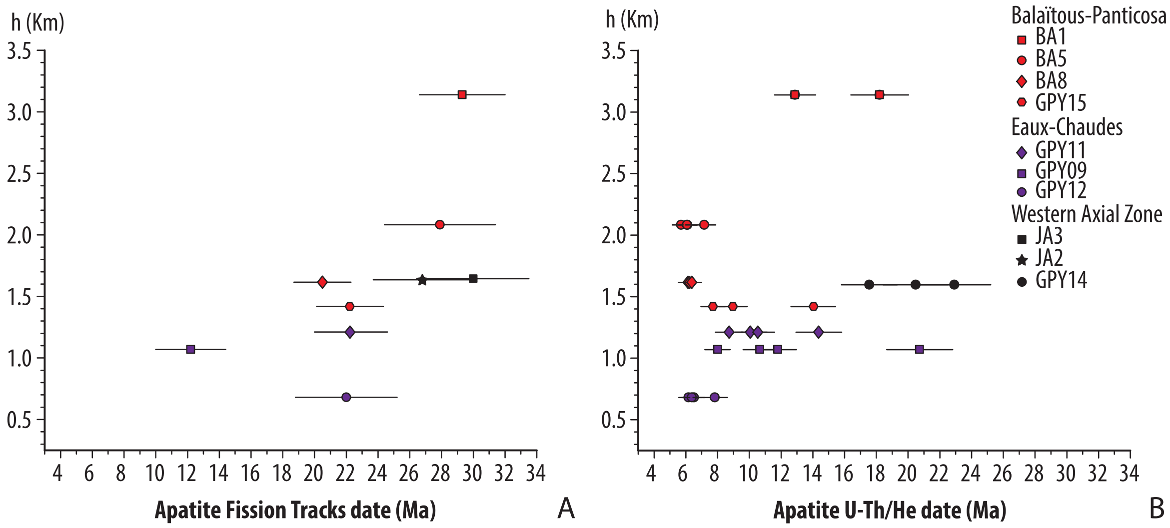
h (Km)
3.5
3.0
2.5
2.0
1.5
1.0
0.5
4 6 8 10 12 14 16 18 20 22 24 26 28 30 32 34
Apatite Fission Tracks date (Ma)
A
h (Km)
3.5
3.0
2.5
2.0
1.5
1.0
0.5
4 6 8 10 12 14 16 18 20 22 24 26 28 30 32 34
Apatite U-Th/He date (Ma)
B
Balaïtous-Panticosa
BA1
BA5
BA8
GPY15
Eaux-Chaudes
GPY11
GPY09
GPY12
Western Axial Zone
JA3
JA2
GPY14

Figure 4

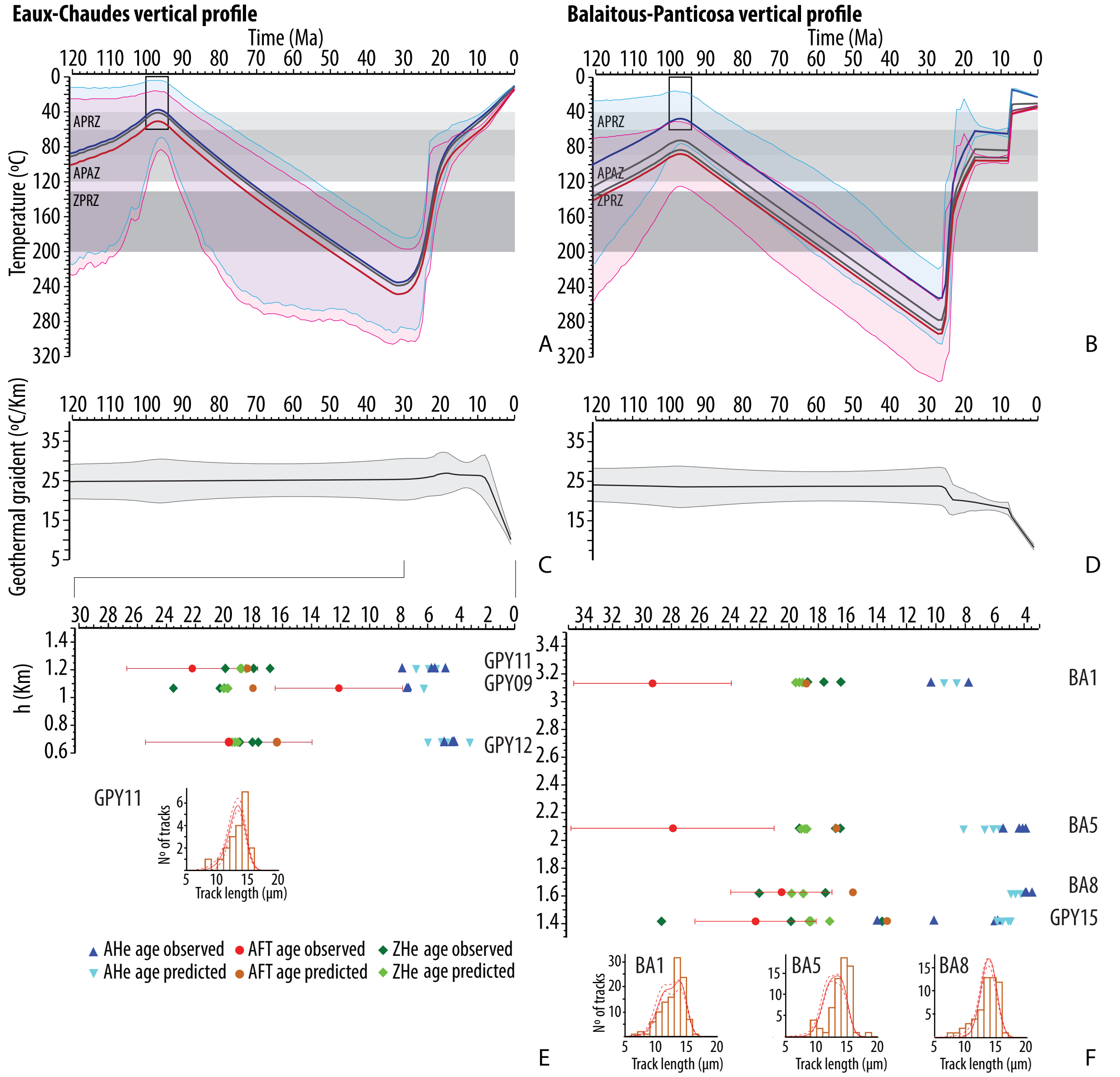

Eaux-Chaudes vertical profile
Balaitous-Panticosa vertical profile
Time (Ma)
Temperature (ºC)
APRZ
APAZ
ZPRZ
A
B
Geothermal graident (ºC/Km)
C
D
h (Km)
GPY11
GPY09
GPY12
BA1
BA5
BA8
GPY15
Nº of tracks
Track length (µm)
AHe age observed
AHe age predicted
AFT age observed
AFT age predicted
ZHe age observed
ZHe age predicted
E
F

Figure 5

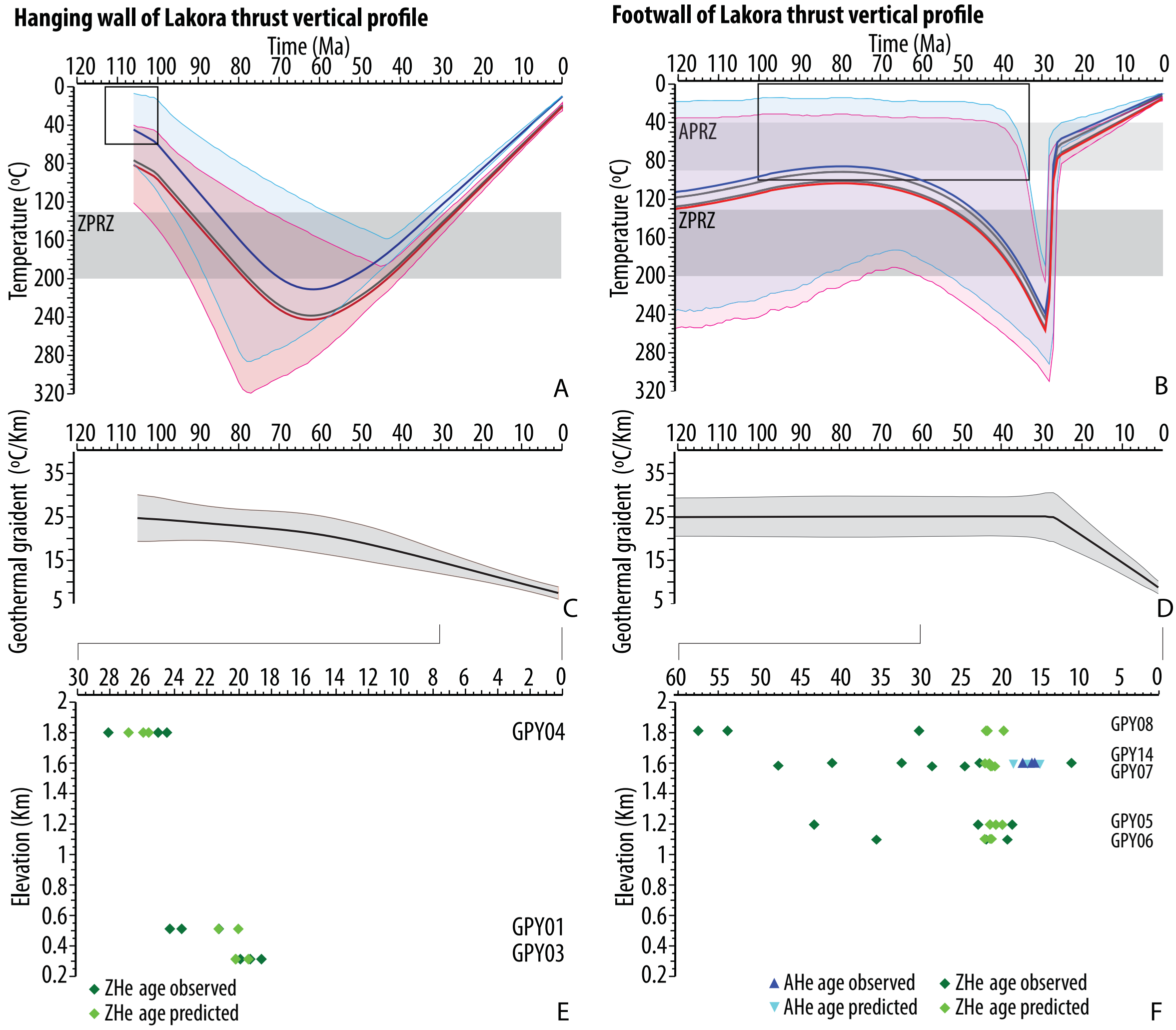

Hanging wall of Lakora thrust vertical profile
Footwall of Lakora thrust vertical profile
Time (Ma)
Temperature (ºC)
ZPRZ
APRZ
A
B
Geothermal graident (ºC/Km)
C
D
Elevation (Km)
GPY04
GPY01
GPY03
GPY08
GPY14
GPY07
GPY05
GPY06
ZHe age observed
ZHe age predicted
AHe age observed
AHe age predicted
E
F

Sample	Latitude (North)	Longitude (East)	Altitude [m]	Nb	ρ_dx 10^4 cm-²	ρ_sx 10^4 cm-²	ρ_i x 10^4 cm-²	[U] [ppm]	$P(\chi^2)$ [%]	Dpar [µm]	Mean track length [µm] (±1 σ) (counted)	Central age [Ma] (±2σ)
Balaitous												
GPY15	42°53'11.2"	00°16'1.00"	1417	24	94.36 (10038)	22.64 (294)	180.2 (2340)	21.96	0	1.4	--	22.23 ± 2.1
[#]BA1	42°50'20.0"	00°17'25.7"	3137	20	141.4 (8282)	22.4 (136)	185.2 (1123)	14.9	42	2.1	13.5 ± 1.9 (56)	29.3 ± 2.7
[#]BA5	42°51'29.1"	00°17'22.2"	2080	20	134.7 (8282)	18.2 (74)	150.8 (611)	13.87	100	1.9	13.9 ± 1.7 (66)	27.9 ± 3.5
[#]BA8	42°45'15.3"	00°14'22.0"	1614	20	138.7 (8282)	24.3 (156)	281.3 (1806)	24.51	98	2.1	13.8 ± 1.9 (114)	20.5 ± 1.8
Eaux-Chaudes												
GPY09	42°53'14.5"	00°25'28.0"	1066	15	99.04 (10038)	12.46 (37)	182.24 (541)	21.66	10	1.1	--	12.2 ± 2.2
GPY11	42°54'34.2"	00°24'36.9"	1208	22	102.4 (10038)	24.18 (121)	190.27 (952)	21.41	15	1.2	13.1 ± 1.6 (20)	22.3 ± 2.3
GPY12	42°57'11.5"	00°26'24.1"	677	13	104.4 (1044)	16.74 (52)	136.82 (425)	14.92	89	1.1	--	22.0 ± 3.2
[#]JA2	42°47'45.5"	00°31'26.8"	1632	20	109.2 (7145)	19.5 (91)	135.8 (634)	17.72	93	--	--	26.8 ± 3.1
[#]JA3	42°47'59.7"	00°31'14.6"	1641	16	112.7 (7373)	41.8 (156)	291 (1087)	32.67	2	--	--	30.0 ± 3.5

Table 1

Table 2

Sample	Latitude (North)	Longitude (East)	Altitude (m)	Nb	^{238}U (μmol)	^{232}Th (μmol)	^{4}He (μmol	Ft	Raw age (Ma) ± 1σ	Corrected age (Ma) ± 1σ	Mean age (Ma) ± 1σ
Balaïtous											
GPY15 1	42°53’11.2”	00°16’1.00”	1417	1	0.42531	0.53135	0.00718	0.727	10.21 ± 0.12	14.04 ±0.16	9.4 ± 4.2
GPY15 3				1	0.32811	0.31242	0.00312	0.676	6.08 ± 0.06	8.99 ± 0.07	(9.3 ± 5.6)
GPY15 4				1	0.13658	0.20121	0.00139	0.765	5.92 ± 0.1	7.74 ± 0.11	
GPY15 5				1	0.11808	0.18527	0.00290	0.669	14.04 ±0.32	20.98 ± 0.46	
BA1 1-3-4	42°50’20.0”	00°17’25.7”	3137	3	0.37182	0.35352	0.00533	0.570	10.4 ± 0.11	18.23 ± 0.17	15.0 ± 3.4
BA1 2-5				2	0.17384	0.21111	0.00225	0.611	7.88 ± 0.11	12.9 ± 0.15	
BA5 6-3	42°51’29.1”	00°17’22.2”	2080	2	1.85155	2.15826	0.01671	0.688	4.22 ± 0.05	6.13 ± 0.06	6.3 ±1.0
BA5 10-8				2	0.79015	0.89596	0.00540	0.702	4.02 ± 0.04	5.73 ± 0.05	
BA5 5-7				2	0.91906	1.05174	0.00665	0.731	4.46 ± 0.04	6.1 ± 0.05	
BA5 1-9				2	0.64933	0.68147	0.00416	0.772	5.54 ± 0.14	7.18 ± 0.05	
BA8 1-3-4	42°45’15.3”	00°14’22.0”	1614	2	0.58653	0.63138	0.00337	0.563	3.59 ±0.04	6.37 ± 0.07	6.27 ± 0.22
BA85-7-8				2	0.64510	0.65350	0.00405	0.633	3.97 ± 0.04	6.26 ± 0.05	
BA8 9				3	0.33613	0.35925	0.00216	0.651	4.02 ± 0.05	6.17 ± 0.07	
Eaux-Chaudes											
GPY09 1	42°53’14.5”	00°25’28.0”	1066	1	0.35513	0.22046	0.00388	0.630	7.44 ± 0.1	11.81 ± 0.15	10.2 ± 6.1
GPY09 2				1	0.25566	0.34676	0.00316	0.685	7.33 ± 0.11	10.69 ± 0.15	(9.4 ±5.0)
GPY09 5-3				2	0.28581	0.21926	0.00468	0.522	10.84 ± 0.14	20.75 ± 0.25	
GPY09 6-4				2	0.40587	0.25853	0.00246	0.514	4.12 ± 0.06	8.01 ± 0.09	
GPY11 1	42°54’34.2”	00°24’36.9”	1208	1	0.33130	0.25048	0.00287	0.603	5.74 ± 0.08	9.52 ± 0.11	10.4 ± 3.0
GPY11 2				1	0.18611	0.19256	0.00163	0.522	5.51 ± 0.09	9.88 ± 0.13	
GPY11 3				1	0.21665	0.32194	0.00290	0.539	7.76 ± 0.11	14.39 ± 0.18	
GPY11 4				1	0.23296	0.21372	0.00173	0.472	4.78 ± 0.09	10.11 ± 0.16	
GPY12 1	42°57’11.5”	00°26’24.1”	677	1	0.41991	1.12264	0.00424	0.735	4.86 ± 0.05	6.61 ± 0.06	6.56 ± 0.78
GPY12 2				1	0.16894	0.40008	0.00140	0.673	4.17 ± 0.07	6.19 ± 0.08	
GPY12 3				1	0.16281	0.39808	0.00141	0.675	4.43 ± 0.08	6.39 ± 0.09	
GPY12 4				1	0.08278	0.27371	0.00079	0.538	4.22 ± 0.12	7.84 ± 0.14	
Western Axial Zone											
GPY14 1-2-6	42°53’57.4”	00°42’57.7”	1594	3	1.22745	1.79027	0.03435	0.691	15.87 ± 0.14	22.94 ± 0.19	20.3 ± 4.3
GPY14 3-4-5				3	1.63647	3.63252	0.04931	0.882	15.51 ± 0.11	17.58 ± 0.12	
GPY14 7-8				2	0.15968	0.41246	0.00557	0.829	17.01 ± 0.19	20.5 ± 0.22	

TABLE 2

Table 3

Sample	Latitude (North)	Longitude (East)	Altitude (m)	^{238}U (ppm)	^{232}Th (ppm)	^{147}Sm (ppm)	^{4}He (nmol/g)	Ft	Ue	Raw age (Ma) ± 1σ	Corrected age (Ma) ± 1σ	Mean age (Ma) ± 1σ
Balaïtous												
GPY15 1	42°53’11.2”	00°16’1.00”	1417	564.3	230.2	18.8	45.9	0.75	617.4	13.75 ± 0.69	18.4 ± 1.47	25.7 ± 6.5
GPY15 2				403.0	47.5	0.5	44.4	0.80	413.9	19.86 ±0.99	25.0 ± 2.00	
GPY15 3				252.3	51.1	0.9	40.9	0.79	264.1	28.67 ± 1.43	36.2 ± 2.89	
GPY15 4				506.6	88.0	0.5	52.8	0.80	526.9	18.56 ±0.93	23.2 ± 1.86	
BA1 1	42°50’20.0”	00°17’25.7”	3137	679.2	106.7	0.5	71.5	0.80	703.7	18.82 ±0.94	23.6 ± 1.89	22.1 ± 1.2
BA1 2				590.8	118.7	0.8	55.4	0.80	618.1	16.59 ±0.83	20.7 ± 1.66	
BA1 3				1040.4	121.1	0.5	102.1	0.81	1068.3	17.71±0.89	21.8 ± 1.75	
BA5 1	42°51’29.1”	00°17’22.2”	2080	667.9	143.8	0.7	73.2	0.79	701.0	19.31±0.97	24.6 ± 1.96	22,2 ± 1.7
BA5 2				318.1	50.7	0.3	30.1	0.79	329.8	16.92 ± 0.85	21.3 ± 1.70	
BA5 3				1125.8	120.3	0.5	103.5	0.80	1153.5	16.61± 0.83	20.8 ± 1.66	
BA8 1	42°45’15.3”	00°14’22.0”	1614	302.6	67.3	0.5	30.1	0.82	318.1	17.53 ±0.87	21.4 ± 1.71	23.7 ± 2.3
BA8 3				163.4	54.3	0.5	21.0	0.85	176.0	22.03 ± 1.10	26.0 ± 2.08	
Eaux-Chaudes												
GPY09 1	42°53’14.5”	00°25’28.0”	1066	768.6	157.5	1.4	87.2	0.82	804.9	20.04 ± 1.0	24.3 ± 1.9	25.8 ± 2.0
GPY09 2				821.6	175.2	1.0	94.7	0.83	862.0	20.32 ± 1.0	24.4 ± 1.9	
GPY09 4				573.7	157.0	3.1	77.6	0.82	609.9	23.52 ± 1.2	28.6 ± 2.3	
GPY11 1	42°54’34.2”	00°24’36.9”	1208	456.0	106.3	1.1	46.7	0.80	480.4	17.99 ±0.9	22.6 ± 1.8	23.1 ± 1.8
GPY11 2				995.8	258.7	0.8	96.1	0.80	1055.4	16.86 ± 0.8	21.2 ± 1.7	
GPY11 3				428.8	109.3	0.7	49.0	0.79	454.0	19.96 ± 1.0	25.4 ± 2.0	
GPY12 1	42°57’11.5”	00°26’24.1”	677	334.3	91.4	1.0	33.9	0.83	355.4	17.67 ± 0.9	21.4 ± 1.7	21.9 ± 0.6
GPY12 2				615.0	143.4	1.9	63.3	0.84	648.0	10.08 ± 0.9	21.5 ± 1.7	
GPY12 3				343.3	112.9	0.6	37.8	0.83	369.3	18.95 ± 0.9	22.7 ± 1.8	
JA3 1	42°47’59.7”	00°31’14.6”	1641	551.2	100.0	1.4	71.8	0.79	574.2	23.16± 1.16	29.4 ± 2.3	196.5± 19.1
JA3 2				124.4	31.2	0.6	14.8	0.78	131.6	20.74± 1.04	26.6 ±2.1	
Western Axial Zone												
GPY01 1	43°02’17.6”	00°44’51.9”	510	131.3	99.9	1.1	17.8	0.70	154.3	21.26± 1.16	30.4 ±2.4	32.0 ± 1.2
GPY01 2				202.4	102.2	0.8	29.7	0.73	226.0	24.29± 1.04	33.2 ±2.7	
GPY01 3				128.9	63.0	8.7	18.3	0.73	143.4	23.56± 2.15	32.3 ± 2.6	
GPY03 1	43°02’29.1”	00°53’50.4”	312	234.8	71.7	0.6	27.1	0.69	251.3	19.94± 1.00	28.8 ± 2.3	28.3 ± 0.8
GPY03 2				125.5	98.9	6.8	15.5	0.67	148.3	19.32± 0.97	28.9 ± 2.3	
GPY03 3				83.2	89.7	1.1	10.5	0.69	103.9	18.63± 0.93	27.1 ±2.2	

Table 3

Table 3 continued

Sample	Latitude (North)	Longitude (East)	Altitude (m)	^{238}U (ppm)	^{232}Th (ppm)	^{147}Sm (ppm)	^{4}He (nmol/g)	Ft	Ue	Raw age (Ma) ± 1σ	Corrected age (Ma) ± 1σ	Mean age (Ma) ± 1σ
Western Axial Zone												
GPY04 1	42°57'08.8"	00°49'57.1"	1800	66.3	52.8	0.3	10.4	0.81	78.5	24.48± 1.22	30.2 ± 2.4	32.6 ± 2.2
GPY04 2				30.3	34.5	0.4	5.2	0.78	38.2	25.04± 1.25	31.9 ± 2.6	
GPY04 3				145.4	107.8	0.5	25.9	0.79	170.2	28.10± 1.41	35.5 ± 2.8	
GPY05 1	42°51'05.4"	00°42'03.9"	1194	156.9	44.2	0.8	38.9	0.78	167.0	43.05± 2.15	55.0 ± 4.4	36.7 ± 13.2
GPY05 2				838.5	583.5	3.4	96.7	0.76	972.8	18.36± 0.92	24.3 ± 1.9	
GPY05 3				552.9	185.4	1.1	72.7	0.73	595.6	22.58± 1.13	30.9 ± 2.5	
GPY06 2	42°49'33.7"	00°42'40.2"	1097	32.6	32.2	0.5	4.1	0.78	40.0	35.24± 0.95	24.2 ± 1.9	25.5 ± 1.3
GPY06 3				58.8	40.2	0.6	8.0	0.81	68.1	18.94± 1.08	26.8 ± 2.1	
GPY07 1	42°56'55.8"	00°50'11.1"	1579	93.9	28.6	2.8	15.4	0.78	100.5	28.30± 1.41	36.3 ± 2.9	34.0 ± 2.3
GPY07 2				88.1	13.0	1.0	11.9	0.76	91.1	24.26± 1.21	31.8 ± 2.5	
GPY08 1	42°54'11.68"	00°48'53.61"	1810	56.9	26.8	0.5	10.2	0.80	63.0	29.97± 1.50	37.5 ±3.0	61.6 ± 17.7
GPY08 2				110.3	77.2	0.6	40.0	0.72	128.1	57.48± 2.87	79.4 ± 6.3	
GPY08 3				45.5	18.2	1.0	14.5	0.79	49.7	53.82± 2.69	67.9 ± 5.4	
GPY14 1	42°53'57.4"	00°42'57.7"	1594	268.4	274.5	2.2	73.5	0.78	331.6	40.79± 2.03	52.4 ±4.2	33.8 ± 14.2
GPY14 2				961.9	384.9	67.3	62.0	0.78	1050.8	10.92± 0.55	14.1 ± 1.1	
GPY14 3				925.9	290.9	5.4	120.4	0.80	992.9	22.44± 1.12	28.1 ± 2.2	
GPY14 4				441.1	112.9	1.5	81.1	0.79	467.1	32.11± 1.61	40.7 ± 3.2	
North Pyrenean Zone												
CTH1 1	43º06'15,9"	00º16'52,0"	439	344.9	124.1	1.3	63.8	0.77	373.5	31.55± 1.58	41.1 ±3.3	43.9 ± 4.1
CTH1 2				362.9	111.7	0.6	67.9	0.79	388.6	32.29± 1.61	40.9 ± 3.3	
CTH1 3				22.6	66.8	0.5	52.5	0.82	237.0	40.93± 2.05	49.7 ± 4.0	
ASS1 1	43º09'10,5"	00º15'09,5"	317	44.6	49.6	1.0	37.6	0.78	56.1	122.51± 6.13	156.7 ± 12.5	219.7 ± 45.1
ASS1 2				148.3	43.6	1.3	180.3	0.80	158.4	206.51± 10.35	2596 ±20.8	
ASS1 3				298.5	192.7	3.9	343.4	0.75	342.9	182.28± 9.11	242.9 ± 19.4	
MCT7 1	43º04'12,9"	00º19'22,7"	778	185.7	78.7	3.1	34.5	0.80	203.8	31.28± 1.56	39.1 ± 3.1	35.8 ± 2.4
MCT7 2				194.4	150.3	4.9	32.5	0.78	229.0	26.19± 1.31	33.4 ± 2.7	
MCT7 3				157.7	21.5	0.6	24.0	0.79	162.7	27.35± 1.37	34.8 ± 2.8	
LBT2 1	43º07'15,6"	00º14'05,7"	367	82.9	46.2	0.8	15.0	0.79	93.5	29.61± 1.48	37.6 ± 3.0	38.4 ± 3.3
LBT2 2				181.6	54.8	0.4	36.6	0.81	194.2	34.82± 1.74	42.8 ± 3.4	
LBT2 3				378.7	98.7	1.4	58.3	0.77	401.4	26.88± 1.34	34.8 ± 2.8	

Table 3 continued

Sample	Latitude (North)	Longitude (East)	Altitude (m)	^{238}U (ppm)	^{232}Th (ppm)	^{147}Sm (ppm)	^{4}He (nmol/g)	Ft	Ue	Raw age (Ma) ± 1σ	Corrected age (Ma) ± 1σ	Mean age (Ma) ± 1σ
North Pyrenean Zone												
NAY3 1	43º10'29,4"	00º17'20,1"	266	130.3	10.6	0.4	87.0	0.81	132.7	120.33± 6.02	148.9 ± 11.9	205.1 ± 49.2
NAY3 2				141.6	32.1	0.9	176.8	0.80	149.0	215.49± 10.77	268.7 ± 21.5	
NAY3 3				113.9	29.2	0.8	103.6	0.79	120.6	157.01± 7.85	197.9 ± 15.8	
GPY17 1	43°01’05.2”	00°24’47.5”	559	174.8	79.4	0.5	22.5	0.75	193.1	21.59± 1.08	28.8 ± 2.3	27.8 ± 1.1
GPY17 3				166.9	57.3	0.6	19.7	0.76	180.1	20.23± 1.01	26.7 ± 2.1	

Annex 1

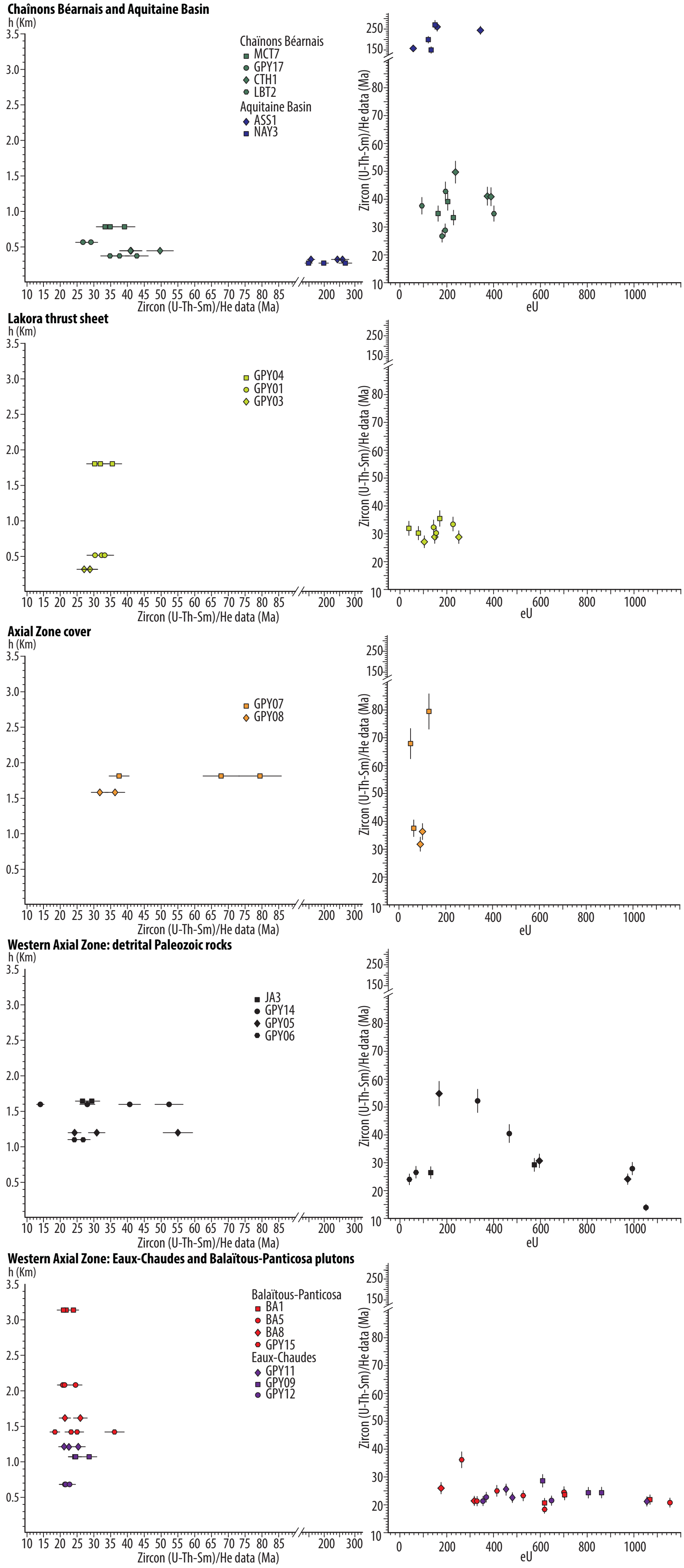
Chaînons Béarnais and Aquitaine Basin
h (Km)
Chaînons Béarnais
MCT7
GPY17
CTH1
LBT2
Aquitaine Basin
ASS1
NAY3
Zircon (U-Th-Sm)/He data (Ma)
eU
Lakora thrust sheet
GPY04
GPY01
GPY03
Axial Zone cover
GPY07
GPY08
Western Axial Zone: detrital Paleozoic rocks
JA3
GPY14
GPY05
GPY06
Western Axial Zone: Eaux-Chaudes and Balaïtous-Panticosa plutons
Balaïtous-Panticosa
BA1
BA5
BA8
GPY15
Eaux-Chaudes
GPY11
GPY09
GPY12